

UC Berkeley

UC Berkeley Previously Published Works

Title

Selective metathesis synthesis of MgCr₂S₄ by control of thermodynamic driving forces

Permalink

<https://escholarship.org/uc/item/1nx397xb>

Journal

Materials Horizons, 7(5)

ISSN

2051-6347

Authors

Miura, Akira
Ito, Hiroaki
Bartel, Christopher J
[et al.](#)

Publication Date

2020-05-11

DOI

10.1039/c9mh01999e

Peer reviewed

Cite this: *Mater. Horiz.*, 2020,
7, 1310Received 11th December 2019,
Accepted 24th February 2020

DOI: 10.1039/c9mh01999e

rsc.li/materials-horizons

Selective metathesis synthesis of MgCr_2S_4 by control of thermodynamic driving forces†

Akira Miura,^a Hiroaki Ito,^b Christopher J. Bartel,^c Wenhao Sun,^{d,e}
Nataly Carolina Rosero-Navarro,^a Kiyoharu Tadanaga,^a Hiroko Nakata,^f
Kazuhiko Maeda^f and Gerbrand Ceder^{cd}

MgCr_2S_4 thiospinel is predicted to be a compelling Mg-cathode material, but its preparation via traditional solid-state synthesis methods has proven challenging. Wustrow *et al.* [*Inorg. Chem.*, 2018, 57, 14] found that the formation of MgCr_2S_4 from $\text{MgS} + \text{Cr}_2\text{S}_3$ binaries requires weeks of annealing at 800 °C with numerous intermediate regrinds. The slow reaction kinetics of $\text{MgS} + \text{Cr}_2\text{S}_3 \rightarrow \text{MgCr}_2\text{S}_4$ can be attributed to a miniscule thermodynamic driving force of $\Delta H = -2 \text{ kJ mol}^{-1}$. Here, we demonstrate that the double ion-exchange metathesis reaction, $\text{MgCl}_2 + 2\text{NaCrS}_2 \rightarrow \text{MgCr}_2\text{S}_4 + 2\text{NaCl}$, has a reaction enthalpy of $\Delta H = -47 \text{ kJ mol}^{-1}$, which is thermodynamically driven by the large exothermicity of NaCl formation. Using this metathesis reaction, we successfully synthesized MgCr_2S_4 nanoparticles (<200 nm) from MgCl_2 and NaCrS_2 precursors in a KCl flux at 500 °C in only 30 minutes. NaCl and other metathesis byproducts are then easily washed away by water. We rationalize the selectivity of MgCr_2S_4 in the metathesis reaction from the topology of the DFT-calculated pseudo-ternary $\text{MgCl}_2\text{-CrCl}_3\text{-Na}_2\text{S}$ phase diagram. Our work helps to establish metathesis reactions as a powerful alternative synthesis route to inorganic materials that have otherwise small reaction energies from conventional precursors.

Introduction

Synthesis is the bedrock of inorganic materials chemistry,¹ serving as the first step to any further investigation into the

New concepts

Complex inorganic materials are usually synthesized by an 'addition' approach, whereby simple precursors are reacted to form a target multicomponent phase. However, if the simple precursors are already very stable themselves, then there may be little free energy left to drive a chemical reaction to a higher-component phase, which often results in slow kinetics and long-lived reaction impurities. Here, we demonstrate that metathesis reactions operate in a fundamentally different synthesis paradigm. During double ion-exchange metathesis, the inclusion of extra chemical species, such as Na^+ and Cl^- , dramatically changes the thermodynamic topology of the phase diagram. This shifting energy landscape modifies the relevant chemical reactions, intensifies reaction thermodynamics, and can relocate the 'thermodynamic sink' of the phase diagram to a new composition—enhancing structure-selectivity towards a target multicomponent phase. We further demonstrate that candidate metathesis reactions can be rapidly screened and evaluated using publicly available DFT thermochemical data. The additional degrees of freedom afforded by including extra elements into the phase diagram opens up a vast and promising design space for creative new metathesis reactions.

structure–property relationships of materials. For ceramic materials, the traditional approach to solid-state synthesis involves grinding or milling precursors into powder form, followed by the firing of these precursors at high temperatures to form more complex materials. While this approach has led to the synthesis of many inorganic materials, it remains limited by a number of thermodynamic and kinetic constraints.² For example, the synthesis temperature should be high enough to facilitate fast diffusion and reaction kinetics, but low enough that the target compound does not melt or decompose. However, high temperatures also lead to the ripening of large particles, which eliminates interfaces and thereby reduces reaction kinetics.³ Because of these often conflicting constraints, solid-state synthesis occasionally proceeds with slow reaction kinetics, non-equilibrium intermediates, or impurities,^{4–6} which hinder the phase-pure synthesis of a desired target material.

One such material that has proven difficult to synthesize via traditional solid-state synthesis is MgCr_2S_4 thiospinel. In the search for Mg-ion cathode materials beyond the dominant Chevrel Mo_6S_8 phase,⁷ Mg-thiospinels emerged as a promising

^a Faculty of Engineering, Hokkaido University, Sapporo 060-8628, Japan.
E-mail: amiura@eng.hokudai.ac.jp

^b Graduate School of Chemical Sciences and Engineering, Hokkaido University,
Sapporo 060-8628, Japan

^c Department of Materials Science and Engineering, UC Berkeley, Berkeley,
California 94720, USA

^d Materials Sciences Division, Lawrence Berkeley National Laboratory, Berkeley,
CA 94720, USA

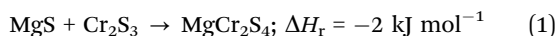
^e Department of Materials Science and Engineering, University of Michigan,
Ann Arbor, Michigan, 48109, USA. E-mail: whsun@umich.edu

^f Department of Chemistry, School of Science, Tokyo Institute of Technology,
Tokyo 152-8550, Japan

† Electronic supplementary information (ESI) available: See DOI: 10.1039/c9mh01999e

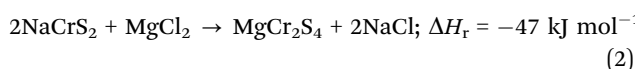
class of compounds. Thiospinels benefit from a soft sulfur anion sublattice, which enhances Mg-ion mobility compared to oxides, and a spinel framework, which provides a favorable tetrahedral \rightarrow octahedral \rightarrow tetrahedral Mg^{2+} migration path with a low diffusion barrier.^{8,9} MgTi_2S_4 was the first demonstrated Mg-thiospinel cathode material, successfully cycled at a C/5 rate at 60 °C and achieving a specific energy density of 230 Wh kg^{-1} .^{10,11} Our computational search for other candidate Mg-thiospinels found MgCr_2S_4 to possess compelling properties, including a high specific capacity (209 mA h g^{-1}) and energy density (244 Wh kg^{-1}), as well as a relatively low Mg-ion diffusion barrier of 540 meV.¹⁰ Notably, MgCr_2S_4 was calculated with density functional theory (DFT) to fall upon the Mg–Cr–S convex hull, meaning it is thermodynamically stable with respect to competing compounds and should therefore be synthesizable.

Following this prediction, Wustrow *et al.* successfully synthesized MgCr_2S_4 through a traditional solid-state synthesis approach—although it was found to be a laborious reaction.¹² Starting from elemental (Mg + Cr + S) precursors, the binary sulfides, MgS and Cr_2S_3 , formed rapidly upon heating. However, the subsequent reaction from $\text{MgS} + \text{Cr}_2\text{S}_3$ to ternary MgCr_2S_4 required holding at 800 °C for two weeks, with numerous intermediate regrinds. Notably, the reaction could not be accelerated by carrying out the synthesis at higher temperatures as MgCr_2S_4 decomposes into MgS and Cr_2S_3 above 900 °C. Although MgCr_2S_4 is indeed a thermodynamically stable compound, we calculate the driving force (reaction enthalpy, ΔH_r) for its formation from $\text{MgS} + \text{Cr}_2\text{S}_3$ to be extremely small (-2 kJ mol^{-1} , eqn (1)).

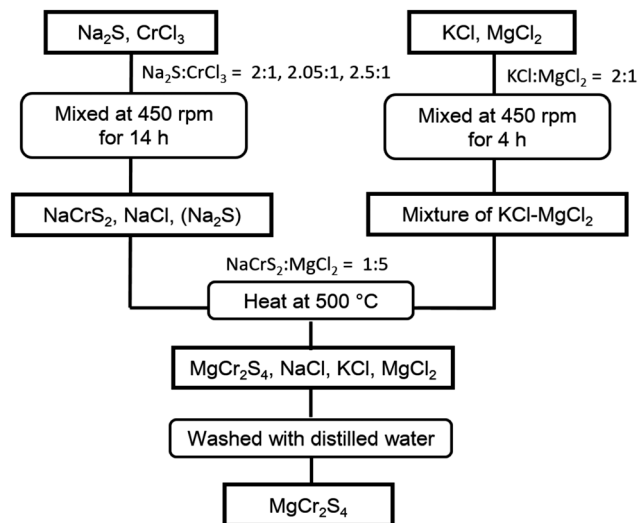


All reaction energies in this work utilize the publicly available DFT-calculated thermochemical data in the Materials Project database (Methods). The slow reaction kinetics observed by Wustrow *et al.* can be attributed to this miniscule thermodynamic driving force. Moreover, long synthesis times can lead to the ripening of large MgCr_2S_4 particles, which reduces the interfacial area needed to activate Mg-ion intercalation and further slows down the reaction kinetics.

Metathesis reactions offer an intriguing synthesis route to solid-state materials with otherwise small reaction energies. In a metathesis reaction, an alkali or alkaline earth metal compound is combined with a metal halide, which drives a highly exothermic double ion-exchange reaction. For example, a compelling metathesis reaction for MgCr_2S_4 can be written as:



The $>20\times$ increase in thermodynamic driving force from $\Delta H_r = -2 \text{ kJ mol}^{-1}$ to -47 kJ mol^{-1} is because Na^+ and Cl^- are separated in the precursors but rejoined to form the very stable NaCl salt on the product side. Along with a dramatic increase in reaction enthalpy, other advantages afforded by metathesis reactions include faster reaction kinetics and the potential to form nanocrystals and porous materials.¹³ Not only can metathesis reactions be used to synthesize stable materials with otherwise small reaction energies, the increased thermodynamic driving force and fast

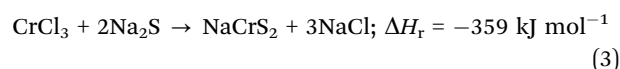


Scheme 1 Two-step metathesis flux synthesis of MgCr_2S_4 .

reaction kinetics also affords the synthesis of metastable materials,¹⁴ as were previously demonstrated on nitrides,^{13,15–17} sulfides,^{13,18,19} and oxides.^{20–22} Motivated by the metathesis reaction shown in eqn (2), we designed a two-step sequential metathesis reaction to synthesize MgCr_2S_4 , as visualized in Scheme 1.

Results

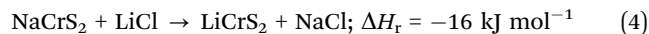
In the first reaction, we ball milled CrCl_3 and Na_2S to form NaCrS_2 (eqn (3)). This reaction is highly exothermic ($\Delta H_r = -359 \text{ kJ mol}^{-1}$) and proceeds even without external heating.



To conduct the metathesis reaction described in eqn (2), we next heated the byproducts from eqn (3) in a KCl– MgCl_2 flux at 500 °C in nitrogen atmosphere. We prepared the KCl– MgCl_2 flux at the eutectic composition of KCl: $\text{MgCl}_2 \sim 2:1$, which has a melting point of $\sim 430 \text{ °C}$.²³

We chose to conduct the reaction in a mixed chloride flux media because the eutectic temperature of a mixed chloride flux can be relatively low, which provides a liquid reaction media to facilitate fast diffusion kinetics. Here, we considered LiCl, NaCl, and KCl as candidate flux chemistries to mix with MgCl_2 . We disqualified a LiCl– MgCl_2 flux because the ion-exchange reaction of NaCrS_2 with LiCl has a favorable driving force to form LiCrS_2 , which could compete with the formation of MgCr_2S_4 (eqn (4)). We also disqualified NaCl– MgCl_2 as a potential flux media because NaCl is a byproduct of the metathesis reaction, meaning the NaCl composition of the flux would change as the metathesis reaction proceeds. Any deviation away from the eutectic composition would increase the melting temperature of the NaCl– MgCl_2 flux; which, if increased too much, could cause the flux to solidify and thereby disrupt the reaction. KCl– MgCl_2 emerges as the ideal flux media, because the formation of KCrS_2 from $\text{NaCrS}_2 + \text{KCl}$ is not thermodynamically

favorable (eqn (5)), and the eutectic point of KCl–MgCl₂ (~430 °C)²³ is lower than that of NaCl–MgCl₂ (~445 °C)²⁴. Furthermore, the formation of NaCl byproduct in a KCl–MgCl₂ flux would actually lower the KCl–MgCl₂ eutectic temperature,²⁴ and thereby would not impede the flux-mediated reaction kinetics.



These reaction thermodynamics are also straightforward to evaluate using the Materials Project Reaction Calculator app, which can help guide the rational design of flux chemistries.

We synthesized NaCrS₂ in a reaction between CrCl₃ and Na₂S by ball-milling at 450 rpm in a zirconia jar with zirconia milling media. We tried three molar ratios for CrCl₃:Na₂S—1:2 (stoichiometric), 1:2.05 (2.5% Na₂S excess), and 1:2.5 (25% Na₂S excess)—producing NaCrS₂ and NaCl (eqn (3)). In the second step, the ball-milled mixture of NaCrS₂ and NaCl were placed in a carbon crucible together with the MgCl₂–KCl flux at a molar ratio of NaCrS₂:MgCl₂ = 1:5. The reaction was performed at 500 °C for 30 minutes in an inert nitrogen atmosphere. After cooling, the synthesized products were washed with distilled water and centrifuged in air to remove the flux and excess MgCl₂ and Na₂S. Fig. 1 shows the XRD characterization of the synthesis products. The ball-milling of Na₂S and CrCl₃ indeed produced NaCrS₂ with NaCl byproduct, as anticipated from eqn (3). The reaction of NaCrS₂ + NaCl in a MgCl₂–KCl flux resulted in MgCr₂S₄, Cr₂S₃ and MgO, where the ratios of these products varied with the Na₂S excess in the precursor (Fig. 1). For a stoichiometric ratio of CrCl₃:Na₂S = 1:2, we observe a coexistence of Cr₂S₃ and MgCr₂S₄. When we include Na₂S excess in the synthesis of NaCrS₂ (eqn (3)), the Cr₂S₃ impurity from the flux reaction is diminished. With 25% Na₂S excess, the reaction yields nearly phase-pure MgCr₂S₄.

All metathesis byproducts and flux media (KCl, NaCl, MgCl₂, Na₂S) and any possibly synthesized MgS are soluble in water and were removed from the system by washing with distilled water. Although our final product yields MgCr₂S₄ as the dominant phase, it contains MgO as a minor impurity. These reactions were conducted in inert nitrogen atmosphere, suggesting the incorporation of oxygen in MgO may have arisen from washing with water. To examine the effect of washing with water, we performed the same synthesis reaction of NaCrS₂ with MgBr₂–KBr flux, with excess MgBr₂ and Na₂S, and subsequently removed metathesis products by washing with anhydrous methanol. In the MgBr₂ synthesis, MgO still forms as an impurity phase, in fact with even larger phase fraction than when synthesized in the MgCl₂–KCl flux (Fig. S1, ESI†). This suggests that the oxygen does not originate from the water. Oxygen impurities may have therefore already existed in the MgCl₂ or MgBr₂ precursors, or from a low but nonzero p_{O₂} and/or p_{H₂O} in the nitrogen atmosphere.

We performed three control experiments to validate the importance of the designed synthesis parameters for the metathesis reaction of MgCr₂S₄. In our first control experiment, we reacted the traditional precursors MgS + Cr₂S₃ in a MgCl₂–KCl flux at 500 °C for 30 min, and in the second control experiment,

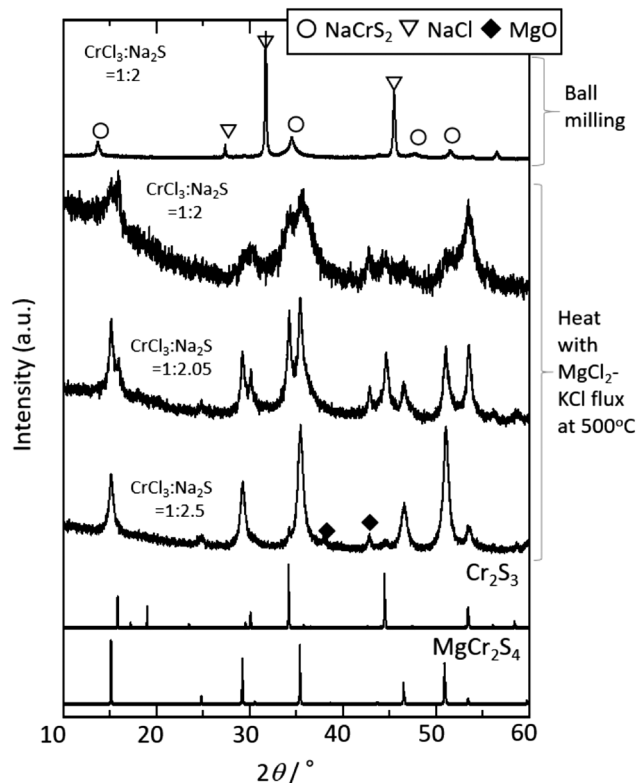


Fig. 1 XRD patterns of NaCrS₂ powder synthesized via ball milling from CrCl₃ and Na₂S, and MgCr₂S₄ powder synthesized by NaCrS₂ and MgCl₂–KCl flux at 500 °C and subsequent wash with water. Different molar ratios of CrCl₃:Na₂S were utilized for producing MgCr₂S₄.

we reacted NaCrS₂ + MgCl₂ without the flux at 500 °C for 30 min. Neither of these two control experiments were found to form MgCr₂S₄ (Fig. S2 and S3, ESI†). The former reaction supports the importance of metathesis precursors, NaCrS₂ + MgCl₂, while the latter reaction supports the need for a liquid phase (*i.e.*, MgCl₂–KCl flux). For the third control experiment, we reacted NaCrS₂ with MgCl₂ at 800 °C, where MgCl₂ becomes liquid even without KCl (the melting point of MgCl₂ is 714 °C).²⁵ This reaction did form MgCr₂S₄, along with Cr₂S₃ impurity (Fig. S3, ESI†). This final control reaction shows that MgCl₂ liquid is important for this reaction, and the presence of KCl enables this liquid phase to form well below the MgCl₂ melting point, decreasing the required temperature from 714 °C to 430 °C. Together, these experiments show that the rapid synthesis of MgCr₂S₄ at 500 °C requires the metathesis precursors (NaCrS₂ + MgCl₂) and the MgCl₂–KCl flux.

Rietveld refinement of MgCr₂S₄ synthesized from Na₂S and MgCl₂ excess (Fig. 2a) shows that the lattice parameter of MgCr₂S₄ is 1.01426(12) nm, agreeing with the previously reported MgCr₂S₄ synthesized by high-temperature solid-state synthesis (1.01415(2) nm).¹² Rietveld refinement shows no inversion between Mg and Cr sites in the spinel structure. Fig. 2b shows the STEM images and corresponding EDX mapping of MgCr₂S₄ particles synthesized via metathesis reactions with Na₂S and MgCl₂ excess. The as-synthesized particles are 50–200 nm in size and 20–50 nm in thickness. The relative surface area of powder

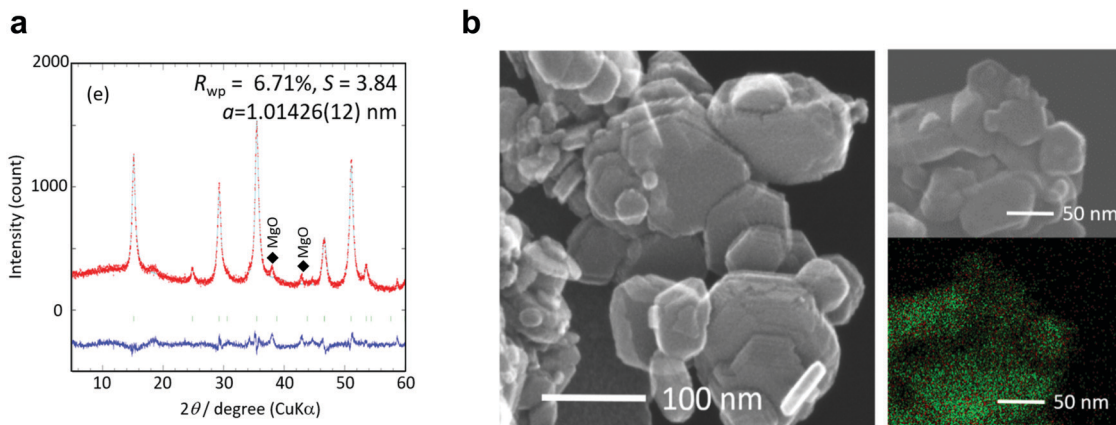


Fig. 2 (a) Rietveld profile of MgCr_2S_4 synthesized with excess Na_2S . Residual is shown as the blue line. (b) STEM image of MgCr_2S_4 platelet particles. Right side is STEM and EDX mapping: red and green signals represent Mg and Cr signals, respectively.

by N_2 absorption is found to be $55 \text{ m}^2 \text{ g}^{-1}$. These small MgCr_2S_4 particle sizes result from the low temperatures and short reaction times of metathesis synthesis, which quench the nanoparticles shortly after nucleation and before significant crystal growth occurs.¹³ This can be contrasted against conventional solid-state synthesis, where high reaction temperatures and long anneal times tend to yield large particle sizes due to Ostwald ripening and particle coarsening during crystal growth.^{3,26} The molar ratio of Mg/Cr/S determined by EDX of the product is 1/2.4/4.1, which is close to the stoichiometric ratio of MgCr_2S_4 . EDX mapping showed homogeneously distributed Mg and Cr, further supporting the formation of MgCr_2S_4 .

The electronic properties of MgCr_2S_4 are an important consideration for Mg-ion battery performance and photochemical applications because Cr_2S_3 has been reported as an n- and p-type semiconductor (band gap, $E_g = 0.8 \text{ eV}$).²⁷ We measured the optical band gap of MgCr_2S_4 using diffuse reflectance spectroscopy (ESI†), which we estimate from the Tauc-plot to be 2.2 eV (Fig. S4, ESI†). By means of Mott-Schottky plot analysis (Fig. S5, ESI†), MgCr_2S_4 is shown to be an n-type semiconductor with a flat-band potential of *ca.* -0.6 V vs. Ag/AgCl at pH 7.0, indicating it is also a candidate H_2 evolution photocatalyst under visible light radiation.²⁸

Discussion

The accelerated formation of MgCr_2S_4 during metathesis (~ 30 minutes) compared with solid-state synthesis (~ 2 weeks) can be rationalized from the thermodynamic topology of each synthesis space. Fig. 3a shows the ternary convex hull phase diagram for Mg–Cr–S, and Fig. 3b shows a pseudo-ternary convex hull phase diagram for MgCl_2 – CrCl_3 – Na_2S , which is a slice of the larger 5-component Mg–Cr–S–Na–Cl phase diagram. The colorbar illustrates the ‘depth’ of the convex hull, corresponding to the reaction energy at each composition relative to the precursor endpoints. Even though MgCr_2S_4 has a very favorable formation enthalpy of $-1.289 \text{ eV atom}^{-1}$, MgS and

Cr_2S_3 also have very negative formation enthalpies of -1.76 and $-1.097 \text{ eV atom}^{-1}$, respectively. In the Mg–Cr–S phase diagram, the deepest point is at the MgS composition, meaning MgS acts as a thermodynamic ‘sink’ in the traditional ceramic synthesis and explains why MgS tends to persist during the traditional ceramic synthesis. Fig. 3c depicts the tiny energy gain to form MgCr_2S_4 along the MgS– Cr_2S_3 reaction tie-line, which further underlies the slow reaction kinetics.

On the other hand, the MgCl_2 – CrCl_3 – Na_2S metathesis phase diagram exhibits a qualitatively different thermodynamic topology. Here, each Mg–Cr–S composition must also be accompanied by a stoichiometrically balanced amount of NaCl, which modifies the reaction energies at each composition in the pseudo-ternary space. MgCr_2S_4 is balanced by 8NaCl, whereas MgS is balanced by 2NaCl, NaCrS_2 by 3NaCl, and Cr_2S_3 by 6NaCl. In the MgCl_2 – CrCl_3 – Na_2S phase diagram, the inclusion of NaCl shifts the deepest thermodynamic point from MgS to $\text{MgCr}_2\text{S}_4 + \text{Cr}_2\text{S}_3$, which are indeed the observed reaction products in Fig. 1 when synthesized without Na_2S excess. The metathesis route therefore enhances the selective synthesis of MgCr_2S_4 by relocating the thermodynamic sink in composition space. Furthermore, because S is tied up with Cr in the NaCrS_2 precursor, MgS is unlikely to form in the metathesis reaction, as this would require NaCrS_2 decomposition and subsequent reaction of S with the MgCl_2 flux.

By increasing the amount of Na_2S excess in the precursor, the diffraction peaks of MgCr_2S_4 became dominant and the Cr_2S_3 impurity is eliminated (Fig. 1). This can be rationalized from Le Chatelier’s principle, as illustrated in Fig. 3c, where Cr_2S_3 impurities react with excess Na_2S as well as excess MgCl_2 from the flux, which further drives the reaction towards the MgCr_2S_4 product side. The reaction between Cr_2S_3 , MgCl_2 and Na_2S (Fig. 3c, orange line) has larger thermodynamic driving force than that between NaCrS_2 and MgCl_2 (Fig. 3c, blue line). Operating with excess Na_2S and MgCl_2 therefore encourages the formation of MgCr_2S_4 at the expense of the Cr_2S_3 impurity. Wustrow *et al.* used a similar strategy in the traditional solid-state synthesis route, providing excess MgS to react with Cr_2S_3 impurities in order to achieve high-purity MgCr_2S_4 .

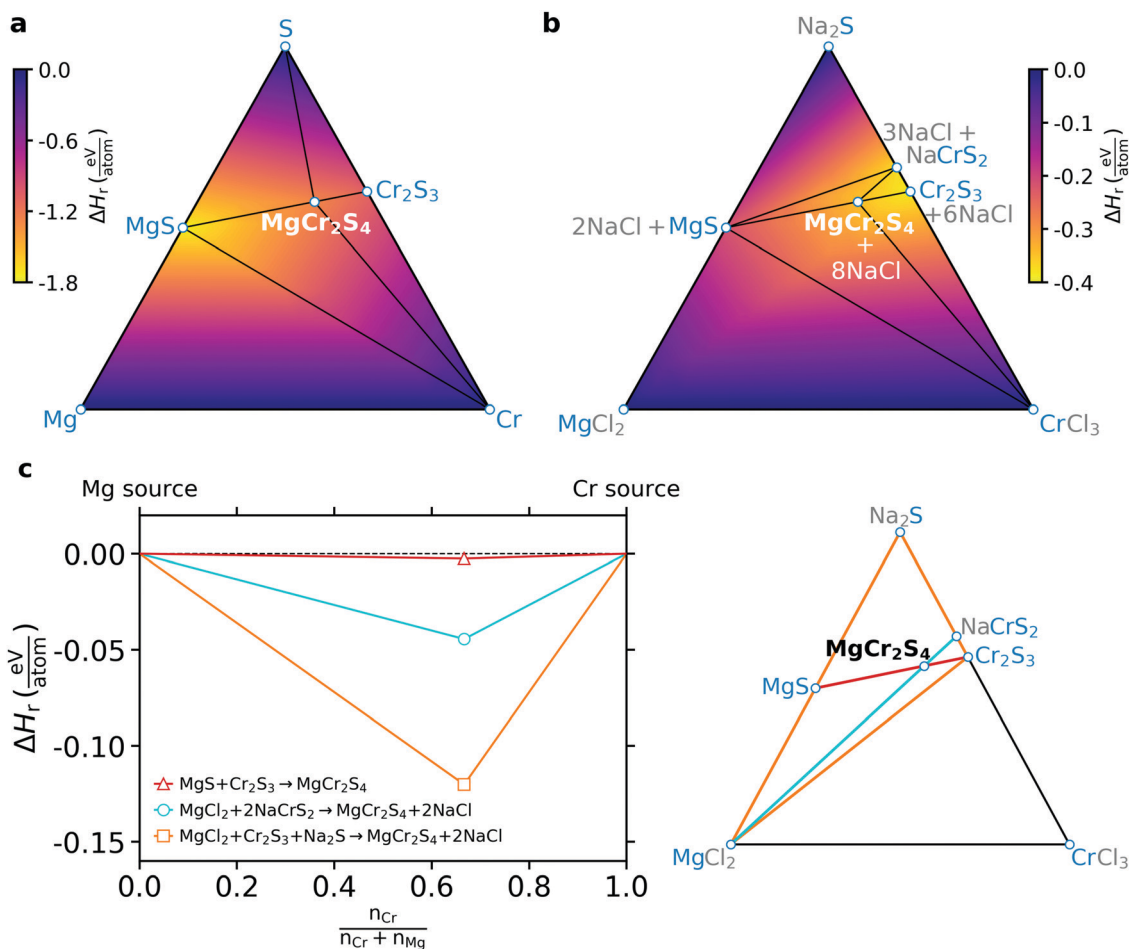


Fig. 3 Ternary phase diagrams for (a) Mg–Cr–S, corresponding to a traditional ceramic synthesis reaction and (b) $\text{MgCl}_2\text{-CrCl}_3\text{-Na}_2\text{S}$, corresponding to a metathesis reaction. The color bar indicates the reaction enthalpy between the corners of each triangle and the convex hull, which represents the minimum energy phase or mixture of phases at each composition. For (b), ΔH_r is calculated by considering the formation of NaCl where appropriate and therefore is a pseudo-ternary representation of the quinary Mg–Cr–S–Na–Cl chemical space. (c) Driving force for MgCr_2S_4 formation from three routes, highlighted by their color in the corresponding pseudo-ternary phase diagram. The reaction relevant to ceramic synthesis (eqn (1)) is shown in red, the metathesis reaction (eqn (3)) is shown in blue, and the reaction that proceeds with excess $\text{Na}_2\text{S} + \text{MgCl}_2$, and consumes impurity Cr_2S_3 , is shown in orange.

Conclusions

In summary, we demonstrated metathesis reactions as a powerful synthesis route to inorganic materials with otherwise small thermodynamic driving forces. The formation of NaCl as a byproduct not only increases the reaction enthalpy of forming the target phase, but shifts the topology of the phase diagram, changing the composition of the deepest point of the convex hull and thereby enhancing structure-selectivity. Here, we demonstrated the metathesis synthesis of MgCr_2S_4 in only 30 minutes at 500 °C, in contrast to a two-week traditional ceramic synthesis at 800 °C with multiple intermediate regrinds. Furthermore, the synthesized MgCr_2S_4 particles were 100–200 nm in size, which is a smaller particle size than would be realized in a direct solid-state ceramic synthesis. Our metathesis synthesis of MgCr_2S_4 enables future studies of its electrochemical performance for Mg-battery and photocatalytic applications.

From a more general perspective, the concept of the metathesis reaction broadens how we evaluate synthesis and synthesizability. Traditionally, we take an ‘addition’ approach to materials synthesis,

where one mixes together simple precursors to form a more complex multicomponent material. In the metathesis route, the reactions are driven by stable but removable byproducts, which include but are not limited to alkali metal halides. For example, the reaction of chlorides/oxides with H_2S or NH_3 gas could also be used to synthesize sulfides, oxysulfides, nitrides and oxynitrides by generating $\text{HCl}/\text{H}_2\text{O}$ gas as a byproduct.^{29–31} Inclusion of these extra species into the phase diagram provides new degrees of freedom for synthesis design, opening up a vast and promising design space for clever metathesis reactions, which can be rapidly screened and evaluated using publicly available DFT thermochemical data. Creative new precursor combinations are still waiting to be exploited within a metathesis synthesis paradigm, which may currently be overlooked due to preconceived notions about precursor selection.³²

Methods

The thermodynamics for all reactions discussed in this work are obtained from density functional theory calculations of the

reaction enthalpy, ΔH_r , as calculated using the Reaction Calculator app on the Materials Project database.³³ The deviation between calculated and experimentally obtained ΔH_r for solid-state reactions, such as those discussed in this work, is expected to be on the order of ~ 5 – 10 kJ mol⁻¹.^{34,35} We note that ΔH calculations do not account for the effects of temperature and entropy on the reaction free energies. For solid-state reactions, the $T\Delta S$ contribution to the free energy is generally negligible when all products and reactants are solids. We demonstrated this by calculating the Gibbs energies of reaction, ΔG_r , at 1000 K for each of the reactions in this work using the model described in ref. 36 (Table S1, ESI†). ΔH_r and ΔG_r (1000 K) are -2 and -9 kJ mol⁻¹, respectively, for eqn (1), and -47 and -50 kJ mol⁻¹ for eqn (2).

The syntheses were performed by two-step metathesis reactions. First, the reaction between CrCl₃ (99%, Sigma-Aldrich) and Na₂S (Nagao & Co., Ltd) with the molar ratio of 1:2, 1:2.05 (2.5% Na₂S excess), and 1:2.5 (25% Na₂S excess) were performed to produce NaCrS₂ and NaCl. This reaction was performed by ball-milling at 450 rpm with zirconia pot and ball. The second step was the reaction of NaCrS₂ with MgCl₂. This reaction was performed at 500 °C for 30 minutes in an inert atmosphere. The ball-milled mixture of NaCrS₂ and NaCl was placed in a carbon crucible together with an MgCl₂-KCl flux: MgCl₂ (99.9%, Kojundo Chemical Laboratory), KCl (>99.5%, Wako Chemicals). The molar ratio of NaCrS₂ to MgCl₂ was 1:5. After cooling, the synthesized products were washed with distilled water and centrifuged in ambient atmosphere to remove flux and excess MgCl₂ and Na₂S. XRD diffraction was measured by MiniFlex 600 (Rigaku). Composition ratio was determined by EDX equipped by scanning electron microscopy (SEM: TM3030). Morphology was observed by scanning transmission electron microscopy (STEM: Hitachi HD-2000). The diffuse reflectance spectra of MgCr₂S₄ were measured using a UV-vis spectrophotometer (JASCO V-750) at room temperature. Mott-Schottky plot measurements were conducted using an ALS760Es electrochemical analyzer (BAS) at room temperature. The electrochemical cell was made of Pyrex glass and was a three-electrode-type system using Pt wire and an Ag/AgCl electrode (in saturated KCl aqueous solution) as the counter and reference electrodes, respectively. The pH of the electrolyte solution was adjusted to be 7.0 by mixing NaH₂PO₄·2H₂O (99.0–102.0%, Kanto Chemical) and Na₂HPO₄·12H₂O (>99.0%, Kanto Chemical), while keeping the total phosphate concentration of 0.1 M.

Conflicts of interest

There are no conflicts to declare.

Acknowledgements

We thank Nagao & Co., Ltd for providing Na₂S. This work was supported as part of the Joint Center for Energy Storage Research (JCESR), an Energy Innovation Hub funded by the U.S. Department of Energy, Office of Science, Basic Energy

Sciences (CJB, WS, GC). This research was partially supported by KAKENHI Grant Numbers JP16H06441 (KM), JP16K21724 (AM), JP17H04950 (AM), and JP19H04682 (AM).

References

- M. G. Kanatzidis, K. R. Poeppelmeier, S. Bobev, A. M. Guloy, S.-J. Hwu, A. Lachgar, S. E. Lattner, R. E. Schaak, D.-K. Seo, S. C. Sevov, A. Stein, B. Dabrowski, J. E. Greedan, M. Greenblatt, C. P. Grey, A. J. Jacobson, D. A. Keszler, J. Li, M. A. Subramanian, Y. Xia, T. Cagin, U. Häussermann, T. Hughbanks, S. D. Mahanti, D. Morgan, D.-K. Seo, N. A. Spaldin, W. E. Buhro, D. E. Giammar, J. A. Hollingsworth, D. C. Johnson, A. J. Nozik, X. Peng, R. L. Bedard, N. E. Brese, G. Cao, S. S. Dhingra, C. R. Kagan, D. B. Mitzi, M. J. Geselbracht, G. C. Lisensky, M. W. Lufaso, P. A. Maggard, O. K. Michael, A. P. Wilkinson, H.-C. zur Loye, T. Egami, J. E. Greedan, J. P. Hodges, J. D. Martin, J. B. Parise, B. H. Toby, T. A. Vanderah, P. C. Burns, J. Y. Chan, A. E. Meyer, C. B. Murray, A. P. Ramirez, M. D. Ward, L. Yu, M. A. Alario-Franco, P. D. Battle, T. Bein, C. L. Cahill, P. S. Halasyamani, A. Maignan and R. Seshadri, *Prog. Solid State Chem.*, 2008, **36**, 1–133.
- F. J. DiSalvo, *Science*, 1990, **247**, 649–655.
- R. M. German, in *Encyclopedia of Materials: Science and Technology*, ed. K. H. J. Buschow, R. W. Cahn, M. C. Flemings, B. Ilshner, E. J. Kramer, S. Mahajan and P. Veysière, Elsevier, Oxford, 2001, pp. 8641–8643.
- D. P. Shoemaker, Y.-J. Hu, D. Y. Chung, G. J. Halder, P. J. Chupas, L. Soderholm, J. F. Mitchell and M. G. Kanatzidis, *Proc. Natl. Acad. Sci. U. S. A.*, 2014, **111**, 10922.
- Z. Jiang, A. Ramanathan and D. P. Shoemaker, *J. Mater. Chem. C*, 2017, **5**, 5709–5717.
- A. S. Haynes, C. C. Stoumpos, H. Chen, D. Chica and M. G. Kanatzidis, *J. Am. Chem. Soc.*, 2017, **139**, 10814–10821.
- D. Aurbach, Z. Lu, A. Schechter, Y. Gofer, H. Gizbar, R. Turgeman, Y. Cohen, M. Moshkovich and E. Levi, *Nature*, 2000, **407**, 724–727.
- Z. Rong, R. Malik, P. Canepa, G. Sai Gautam, M. Liu, A. Jain, K. Persson and G. Ceder, *Chem. Mater.*, 2015, **27**, 6016–6021.
- M. Liu, Z. Rong, R. Malik, P. Canepa, A. Jain, G. Ceder and K. A. Persson, *Energy Environ. Sci.*, 2015, **8**, 964–974.
- M. Liu, A. Jain, Z. Rong, X. Qu, P. Canepa, R. Malik, G. Ceder and K. A. Persson, *Energy Environ. Sci.*, 2016, **9**, 3201–3209.
- X. Sun, P. Bonnicksen, V. Duffort, M. Liu, Z. Rong, K. A. Persson, G. Ceder and L. F. Nazar, *Energy Environ. Sci.*, 2016, **9**, 2273–2277.
- A. Wustrow, B. Key, P. J. Phillips, N. Sa, A. S. Lipton, R. F. Klie, J. T. Vaughney and K. R. Poeppelmeier, *Inorg. Chem.*, 2018, **57**, 8634–8638.
- J. B. Wiley and R. B. Kaner, *Science*, 1992, **255**, 1093–1097.
- W. Sun, S. T. Dacek, S. P. Ong, G. Hautier, A. Jain, W. D. Richards, A. C. Gamst, K. A. Persson and G. Ceder, *Sci. Adv.*, 2016, **2**, e1600225.
- J. Odahara, W. Sun, A. Miura, N. C. Rosero-Navarro, M. Nagao, I. Tanaka, G. Ceder and K. Tadanaga, *ACS Mater. Lett.*, 2019, **1**, 64–70.

- 16 A. Miura, C. Rosero-Navarro, Y. Masubuchi, M. Higuchi, S. Kikkawa and K. Tadanaga, *Angew. Chem., Int. Ed.*, 2016, **55**, 7963–7967.
- 17 E. G. Rognerud, C. L. Rom, P. K. Todd, N. R. Singstock, C. J. Bartel, A. M. Holder and J. R. Neilson, *Chem. Mater.*, 2019, **31**, 7248–7254.
- 18 A. J. Martinolich, J. A. Kurzman and J. R. Neilson, *J. Am. Chem. Soc.*, 2016, **138**, 11031–11037.
- 19 A. J. Martinolich and J. R. Neilson, *Chem. Mater.*, 2017, **29**, 479–489.
- 20 R. D. Shannon, D. B. Rogers and C. T. Prewitt, *Inorg. Chem.*, 1971, **10**, 713–718.
- 21 P. K. Todd and J. R. Neilson, *J. Am. Chem. Soc.*, 2019, **141**, 1191–1195.
- 22 P. K. Todd, A. M. M. Smith and J. R. Neilson, *Inorg. Chem.*, 2019, **58**, 15166–15174.
- 23 O. Menge, *Z. Anorg. Chem.*, 1911, **72**, 162–218.
- 24 E. Jänecke, *Z. Anorg. Chem.*, 1950, **261**, 213–225.
- 25 D. R. Lide, *CRC Handbook of Chemistry and Physics, 84th Edition*, CRC Press, 2003.
- 26 L. Ratke and P. W. Voorhees, *Growth and Coarsening: Ostwald Ripening in Materials Processing*, Springer-Verlag, 2002.
- 27 A. Anedda, E. Fortin, F. Ledda and A. Serpi, *Phys. Status Solidi B*, 1982, **114**, K143–K146.
- 28 K. Maeda, R. Abe and K. Domen, *J. Phys. Chem. C*, 2011, **115**, 3057–3064.
- 29 S. H. Elder, L. H. Doerrer, F. J. Disalvo, J. B. Parise, D. Guyomard and J. M. Tarascon, *Chem. Mater.*, 1992, **4**, 928–937.
- 30 A. Miura, K. Tadanaga, E. Magome, C. Moriyoshi, Y. Kuroiwa, T. Takahiro and N. Kumada, *J. Solid State Chem.*, 2015, **229**, 272–277.
- 31 H. Kageyama, K. Hayashi, K. Maeda, J. P. Attfield, Z. Hiroi, J. M. Rondinelli and K. R. Poeppelmeier, *Nat. Commun.*, 2018, **9**, 772.
- 32 X. Jia, A. Lynch, Y. Huang, M. Danielson, I. Lang'at, A. Milder, A. E. Ruby, H. Wang, S. A. Friedler, A. J. Norquist and J. Schrier, *Nature*, 2019, **573**, 251–255.
- 33 A. Jain, S. P. Ong, G. Hautier, W. Chen, W. D. Richards, S. Dacek, S. Cholia, D. Gunter, D. Skinner, G. Ceder and K. A. Persson, *APL Mater.*, 2013, **1**, 011002.
- 34 C. J. Bartel, A. W. Weimer, S. Lany, C. B. Musgrave and A. M. Holder, *npj Comput. Mater.*, 2019, **5**(1), 4.
- 35 G. Hautier, S. P. Ong, A. Jain, C. J. Moore and G. Ceder, *Phys. Rev. B: Condens. Matter Mater. Phys.*, 2012, **85**(15), 155208.
- 36 C. J. Bartel, S. L. Millican, A. M. Deml, J. R. Rumpitz, W. Tumas, A. W. Weimer, S. Lany, V. Stevanovic, C. B. Musgrave and A. M. Holder, *Nat. Commun.*, 2018, **9**, 4168.